Bulletin of Earthquake Engineering
https://doi.org/10.1007/s10518-024-01871-7

ORIGINAL ARTICLE

Performance-based versus conventional seismic design: comparative assessment on a 4-story RC moment frame

Akrivi Chatzidaki[1] · **Dimitrios Vamvatsikos**[1] · **Enrique Hernández-Montes**[2]

Received: 28 June 2023 / Accepted: 24 January 2024

Abstract
Five different design approaches are compared on a single mid-rise reinforced concrete building, pitting two performance-based designs against three conventional methods in delivering a solution that satisfies different sets of performance objectives. Two of the conventional designs stem from the literature, and they represent 2003 IBC compatible solutions. Another employs the yield point spectra to deliver a code-like solution, satisfying the design norms without needing iterations. The final two are based on the yield frequency spectra to offer a design that can satisfy more detailed performance objectives in a single step. Overall, all five methods are shown to deliver what is expected. Conventional methods can safely capture the code requirements, yet they are disadvantaged when treading in beyond-life-safety territory, where Immediate Occupancy or Collapse Prevention objectives cannot be easily satisfied, a problem that is not shared by performance-based approaches.

Keywords Performance-based earthquake engineering · Uncertainty · Fragility · Demand · Capacity

1 Introduction

Seismic design is an inherently complex process that is arguably far more iterative than the process of structural assessment, heavily compounded by the fact that in the former case we start with a general configuration in need of sizing (or even configuring), while in the latter we have an already-designed structure to assess (see also relevant discussions in O'Reilly and Calvi 2019). Thus, design is practically never direct, as it actually comprises multiple cycles of re-design and re-analysis to conform to required performance objectives (POs). How one defines such objectives and then goes about meeting them characterizes both the approach and its end result (e.g., Vamvatsikos et al. 2016a, b).

✉ Akrivi Chatzidaki
cakrivi@central.ntua.gr

[1] Institute of Steel Structures, School of Civil Engineering, National Technical University of Athens, Athens, Greece

[2] Department of Civil Engineering, University of Granada, Granada, Spain

In terms of the definition of POs, risk versus intensity basis are the two options. In both cases, one is interested in constraining the undesirable event of demand, D, exceeding capacity, C, where both are typically defined in terms of engineering demand parameters (EDPs), such as member forces, moments, or deformations. In risk-based/targeted design, or performance-based seismic design (PBSD, Krawinkler et al. 2006; Franchin and Pinto 2012; Sinković et al. 2016; Franchin et al. 2018; Kazantzi and Vamvatsikos 2021), of interest is the mean annual frequency (MAF) of $D > C$, or $\lambda(D > C)$. Then, meeting a PO means that the $x\%$ percentile (i.e., $x\%$ confidence-level) estimate of $\lambda(D > C)$ due to additional uncertainty from modeling, analysis, material properties etc. is lower than the associated tolerable MAF of the PO, λ_{PO}:

$$\lambda_{x\%}(D > C) < \lambda_{PO} \tag{1}$$

Risk-based design methodologies allow setting any number of POs and designing the structure in order to satisfy them within constraints imposed by e.g., architectural considerations. At their most advanced form, specific (non-)exceedance rates of more sophisticated decision variables can be targeted, such as monetary losses, casualties etc. (Shahnazaryan and O'Reilly 2021; Shahnazaryan et al. 2022; Gentile and Calvi 2023).

Intensity-based design is practically much simpler. Therein, satisfying an objective is reduced to directly checking for a conservative (i.e., high) estimate of the EDP demand exceeding a conservative (i.e., low) estimate of the capacity at a single intensity measure (IM) level, or IM_O, provided by a design spectrum associated with a given exceedance MAF, typically associated with an exceedance probability of 10% in 50yrs (henceforth noted 10%/50yrs):

$$D_{z\%}\left(IM_O\right) > C_{(1-w)\%} \tag{2}$$

z, w are confidence levels (greater than 50%) that are chosen to indirectly achieve the required safety (e.g., Ravindra and Galambos 1978; Ellingwood et al. 1982; Sørensen et al. 1994); they are typically expressed via demand-increasing and capacity-reducing multipliers, i.e., load and resistance safety factors, and form the basis of modern codes (e.g., CEN 2005; ASCE 2010).

The elegance of Eq. (2) is rather marred by the (typically unavoidable) structural nonlinearity. To incorporate the beneficial effects of ductility without invoking nonlinear analysis, a response modification (strength reduction) factor, R, or behaviour factor, q, is applied on the elastic demands. These factors are approximately estimated for classes of structures, but they actually depend on each building's characteristics, such as the ductility capacity, overstrength and redundancy, properties that are not known a priori, as well as the period or the height of the structure, which are known design parameters with imperfectly known effects on performance. Intensity-based seismic design typically intends to achieve a single PO at one seismic hazard level, that is Life Safety (LS), simply by ensuring that critical members have sufficient strength and conform with the detailing requirements. Serviceability is also addressed by limiting interstory drifts either under the design lateral loads or for a reduced design spectrum corresponding to a more frequent hazard level. Although compliance with other limit-states such as Global Collapse is often claimed in codes, this is not explicitly checked for, but only implicitly "guaranteed" by the aforementioned process. In other words, intensity-based design is an inherently inaccurate approach (see Iervolino et al. 2018; Aschheim et al. 2019) as it bypasses a rigorous assessment.

Such a performance assessment is best conducted by assessing $\lambda(D>C)$ for the PO at hand. It can be obtained by cointegrating the system fragility curve associated with the given threshold of interest, with the seismic hazard curve:

$$\lambda(D > C) = \int \mathrm{P}[D > C|IM] \cdot |\mathrm{d}\lambda(IM)| \tag{3}$$

where $\mathrm{P}[D>C \mid IM]$ is the probability of D exceeding C given the IM, also known as the fragility curve, while $|\mathrm{d}\lambda(IM)|$ is the differential of the seismic hazard curve. Without doubt, the process of assessment comes with its own complications, as it would optimally require a detailed nonlinear model and multiple response history analyses.

Given that the relationship between the design variables and the target POs is not invertible, one cannot design directly for specified POs. Thus, risk-based design inevitably becomes an iterative approach of re-design and re-assessment. Several approaches have been proposed to guide such iterations. Arguably, the most comprehensive ones require the user to work with the full structure, choosing the needed structural adjustments either using experience and intuition (e.g., Krawinkler et al. 2006; Zareian and Krawinkler 2012) or via formal numerical optimization (e.g., Fragiadakis and Lagaros 2011; Franchin and Pinto 2012). On the other hand, using a single-degree-of-freedom proxy and adopting a design-invariant term is by far the most practical and popular approach for conducting design iterations (Vamvatsikos et al. 2016a, b; Shahnazaryan and O'Reilly 2021).

In this matter, adopting a period versus a displacement basis are the two mainstream proposals. The design methods proposed in current codes rely upon an initial estimation of the structural period (period/force-based approaches). However, the lateral strength and stiffness of a structure change in subsequent re-design and re-analysis cycles, leading to significant period changes. Chopra and Goel (2000) have highlighted the difficulty of accurately estimating the fundamental period of the final design after examining a large number of buildings in California. The inaccuracy of the period estimate may increase the number of iterations, hampering intensity-based approaches, but even more so risk-based ones.

On the other hand, multiple researchers such as Priestley (2000) and Aschheim (2002) suggested that the yield displacement is a more stable parameter that can be estimated early in the design process. Taking advantage of its stability, they proposed using yield displacement instead of the fundamental period as a basis for estimating the design base shear (displacement-based approaches), aiming to significantly reduce the number of re-design and re-analysis iterations required. On such basis, multiple displacement-based design procedures have been proposed, e.g., Moehle (1992); Aschheim and Black (2000); Priestley et al. (2008); Hernández-Montes et al. (2023); da Silva et al. (2023). Of essence in reducing the number of iterations is to obtain a good estimate of the yield displacement, which is considered a relatively easy task given that it mainly depends on the known geometry and material properties rather than the unknown building strength. Still, conventional displacement-based approaches remain anchored on the intensity-basis rather than a performance/risk-basis, thus they deliver solutions without any explicit guarantee of meeting specific POs (Vamvatsikos et al. 2016a, b; Vamvatsikos 2017; O'Reilly and Calvi 2020; Van der Burg et al 2022).

In the following, to test the capabilities of different design approaches, we shall pit three intensity-based and two risk-based designs against each other, using a four-story reinforced concrete (RC) office building as a testbed. Two of the intensity-based designs stem from literature and are period-based designs, while the third one is a displacement-based design that relies upon the use of the Yield Point Spectra (YPS) proposed by Aschheim and Black

(2000). Regarding the risk-based designs, they both rely on the use of the Yield Frequency Spectra (YFS, Vamvatsikos and Aschheim 2016) as the design tool, and they are either based on a code-like approximation of the seismic hazard or on actual site-specific seismic data.

2 Case-study building

The case-study is a four-story RC office building, representative of the mid-rise offices constructed in the highly seismic region in coastal California. It is a benchmark building originally designed by Haselton et al. (2008). It has two perimeter moment-resisting frames (MRFs) acting in each principal direction as its lateral-load resisting system and internal columns that carry only the gravity loads. Each MRF has four bays of 30ft (9.1 m) resulting in a total length of 120' (36.6 m), as shown in Fig. 1a. The building has a standard floor plan configuration of 180' × 120' (54.8 × 36.6 m) dimensions, as presented in Fig. 1b, while its height is 54' (16.5 m) with a first story of 15' (4.6 m) and 13' (4.0 m) height on the remaining ones. Dead load of 175psf (8.4 kN/m^2) and live load of 50psf (2.4 kN/m^2) are assumed for the design, with the latter not acting on the roof. Concrete and steel rebars of characteristic strength equal to f_{ck} = 5ksi (35 MPa) and f_{ck} = 60ksi (414 MPa), respectively, are used for the beams and columns, while the two-way flat post-tensioned slab has 8″ (0.2 m) thickness.

3 MRF design approaches

The five different design approaches that were followed for designing the MRFs are herein named as CA, CB, MA, MB and MC. CA and CB frames are designed by (Curt) Haselton et al. (2008) following code-compatible intensity-based design procedures that rely upon an initial estimation of the fundamental period of the structure (i.e., period-based). MA, MB and MC moment-frames are designed by (Mark) Aschheim et al. (2019), the former following an intensity-based design procedure based on an initial estimation of the yield

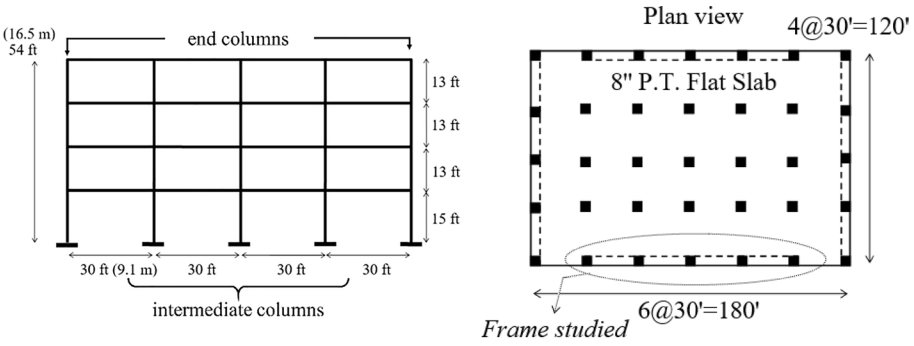

Fig. 1 Four-story reinforced concrete building: **a** elevation of the perimeter moment resisting frame and **b** plan view of a typical story (adopted from Aschheim et al. 2019)

displacement through YPS, while the other two are designed by more advanced risk-based approaches via YFS by maintaining a constant yield displacement basis.

4 Theoretical background

4.1 Intensity-based design via YPS

The YPS are constant ductility spectra calculated using the elastic response spectrum of the code as a basis; thus, designing via the YPS offers performance compatible to current codes. The YPS approach requires an initial estimation of the yield displacement, δ_y^*, of the equivalent single degree of freedom (SDOF) system that serves as a proxy of the full structure. Having established δ_y^* (or its full-structure equivalent δ_y) and the target response of the structure in terms of allowable system ductility, the base shear strength at yield, V_y^*, of the equivalent SDOF can be directly determined through the YPS. Based on V_y^*, the required period of the structure and the cross-sectional dimensions and reinforcement of the RC members are determined e.g., via plastic mechanism analysis. Having established the cross-sectional characteristics, the new yield displacement is estimated and if an iteration is required in case of discrepancies vis-à-vis the initial estimate, the aforementioned process is repeated. This design approach is meant to reduce the number of required design-analyses cycles while remaining compatible to current codes; still, it does not explicitly account for uncertainties.

4.2 Risk-based design approach through the YFS

Risk-based design approaches deliver structural solutions that satisfy a set of any number of POs that are defined a priori by the analyst. The YFS (Vamvatsikos and Aschheim 2016) offers a means for such a design by employing an equivalent SDOF proxy of the full structure and explicitly linking the MAF of exceeding any displacement value of interest with V_y^* of the SDOF. It relies upon the stability of the yield displacement despite changes in the system's strength, thus strength variations estimated via the YFS are related to changes in the period of vibration and the lateral stiffness of the structure. In YFS applications the desired POs are thus expressed in terms of the allowable MAF of exceeding specific global ductility or displacement limits at a desired level of confidence, while the maximum strength V_y^* required to fulfill the POs, as obtained through the YFS, is the one that governs the structural design. Having established V_y^* and converted it back to the multi-degree-of-freedom (MDOF) system, a mechanism design analysis can be followed to establish the required strength and stiffness of individual members.

Apart from the estimate on the yield displacement, the YFS also requires an assumption on the force–deformation backbone of the SDOF model as well as comprehensive information on the seismic hazard of the site. The backbone is used for estimating the building's fragility curve, either through a series of nonlinear dynamic analyses or by economizing though approximate R–μ–T (strength reduction-ductility-period) relationships, preferably ones that provide the entire distribution of the response (e.g., Vamvatsikos and Cornell 2006; Ruiz-Garcia and Miranda 2007; Bakalis et al. 2019). The obtained fragility curves are cointegrated with the site hazard curve to obtain the YFS. Regarding the seismic hazard, it needs to be provided for (pseudo-)spectral acceleration, $Sa(T)$, at multiple values of the period T. Such information is optimally derived for the site of interest for via

probabilistic seismic hazard analysis (Cornell 1968). If such information is not available, the code elastic design spectra (or uniform hazard spectrum, UHS) can be used instead, by adopting an approximation of the logarithmic slope of the hazard curve, k, that allows extrapolating to other hazard levels per Cornell et al. (2001). In this case, some conservatism may be introduced to the YFS estimate, especially if the UHS is extrapolated to very frequent or very rare events.

Both the YPS and YFS rely upon the equivalent SDOF approximation, thus some inaccuracies can be introduced when designing MDOF structures. For this reason, some refinement of the initial design may be required in case of POs that do not correlate well with the SDOF response, such as more localized responses of interstory drift or floor acceleration that are affected by higher modes.

4.3 Treatment of unmodeled uncertainty and confidence level estimates

There are inherent uncertainties in assessment, ranging from the values assumed for (non-deterministic) model parameters such as the yield strength, mass, stiffness etc., to the choice of the model itself, and the method adopted for the analysis. Theoretically, these can be incorporated by explicitly taking into account their influence when modeling/assessing the structure, assigning probability distributions and an associated correlation structure to influential uncertain parameters and assessing their effect, e.g., via Monte Carlo simulation (e.g., Dolsek 2009; Liel et al. 2009; Vamvatsikos and Fragiadakis 2010; Gokkaya et al. 2016). However, this would require a significant number of analyses at a heavy computational expense (e.g., Vamvatsikos 2014). As a more cost-effective solution, such additional unmodeled sources of uncertainty are only approximately considered a posteriori, introducing variability in the performance assessment results, which are no longer deterministic but instead they become uncertain, following a distribution of their own.

For lack of a better (or more cost-effective) option, one typically assumes that by employing the central values (means or medians) for the unmodeled random variables, the central value of the estimated output distribution can be accurately captured; thus the results of one's assessment are assumed to be unbiased. However, the dispersion in the results is surely impacted since in most cases adding more random variables (i.e., noise) to the problem results in increasing the uncertainty of the output. The theoretically "simplest" way to account for this additional uncertainty, β_ε, would be to estimate its value and inject it back to the outputs. Of course, to do so accurately requires considerable experience and/or non-negligible expense. One can instead employ canned literature values (e.g., FEMA 2009a, 2012), keeping in mind that, as a general rule, β_ε should be lower than the dispersion obtained by the modelled sources of uncertainty, otherwise the aforementioned assumption of unbiasedness may be suspect.

Having established β_ε, one has two options to incorporate it in the performance assessment. The first one is to aggregate the dispersion obtained by the modelled variables with the additional model error dispersion through the square root of the sum of squares (SRSS) rule, following the so-called first-order assumption (Cornell et al. 2001). In this case both sources of uncertainty are treated equally and we are not able to distinguish the variance from each source; still, this approach is simple and can be easily implemented in practice. Alternatively, one can employ the additional model error dispersion separately from the modelled one and define multiple realizations of the output distribution, each of them being a copy of the initial distribution with a shifted mean representing the error in the

obtained estimate. In both cases though, such added variability in the results of the analysis offers a new twist to the discussion of what $D > C$ really means in Eq. (1) to (3).

To better present our case, let us consider two virtual safety-checking examples (as they are more intuitive than the inverse of exceedance-checking) for $D < C$, namely $99 < 100$ versus $50 < 100$. If the values of demand and capacity are deterministic without incorporating any uncertainty, then both inequalities would be satisfied as they are valid from a mathematical standpoint. In other words, we should be safe in both cases. However, given the multiple sources of uncertainty, neither D nor C are deterministic. This results in an uncertainty on the outcome of whether exceedance has taken place. For our examples, given similar levels of uncertainty, the $50 < 100$ case should be preferred over the $99 < 100$ one since the difference between D and C is higher, thus imparting greater *confidence* on the results of the inequality. Consequently, the degree of confidence on the design/analysis outputs highly depends on their dispersion due to the inherent uncertainties.

Despite the need of assigning desired confidence levels for checking, intensity-based design approaches cannot directly account for them, since they either ignore randomness in the input data, or, when they account for it, they only do so approximately. In such cases where confidence is not defined otherwise, the confidence level of 50% is assumed and is also propagated to performance assessment for consistency purposes. On the contrary, designing using risk-based approaches, and especially YFS, allows explicit consideration of uncertainty since user-selected confidence levels can be enforced on the target POs. The confidence level assigned to each PO should be dependent on the consequences associated with each type of failure. For instance, the highest confidence level should be assigned to failures related to loss of the load-carrying capacity of the structure, especially if such failures are associated with progressive collapse. A lower value of confidence can be applied to failures of lesser consequences. Of course, higher confidence in achieving a PO generally requires a stricter design and comes at a greater cost.

5 Case-study building designs

5.1 Design of the CA and CB frames

The CA and CB frames were designed by Haselton et al. (2008) for a site matching San Jose, California (latitude = 37.33659º, longitude = −121.89056º) on Site Class D soils. Specifically, the ASCE 7–10 (ASCE 2010) hazard spectrum with 2% probability of exceedance in 50 years (henceforth referenced as 2%/50yrs) has the values of $S_{MS} = 1.50$ g and $S_{M1} = 0.90$ g, while the smoothed design spectrum according to ASCE 7–10 for the 10%/50yrs is based on $S_{DS} = 2/3(S_{MS}) = (2/3)\cdot(1.50\text{ g}) = 1.00$ g and $S_{D1} = (2/3)\cdot(S_{M1}) = (2/3)\cdot(0.90\text{ g}) = 0.60$ g.

The provisions of the International Building Code 2003 (ICC 2003) are adopted for CA and CB frames, thus a typical code-compatible period-based design procedure is followed. The difference between these two approaches is that the CA frame is designed following common practitioner-design practices, thus exceeding the minimum code requirements. On the contrary, the CB frame meets code provisions as closely as possible to their minimum values. More details on the design approaches adopted for these two frames can be found in Haselton et al. (2008). The cross-sectional dimensions and reinforcement for beams and columns of the perimeter MRFs are listed in Table 2 without including any additional

small diameter rebars used for supporting stirrups and to satisfy minimum rebar distance requirements.

5.2 Design of the MA frame

The MA frame is designed as per Hernández-Montes and Aschheim (2019), following an intensity-based design procedure that is based on the stability of the yield displacement through the YPS. The YPS is determined using the smoothed response spectrum of ASCE 7–10 (ASCE 2010) for the San Jose site as a basis.

Designing using the YPS seeks performance compatible to the one obtained in current codes, thus performance requirements comparable to those in ASCE 7–10 are targeted. Specifically, ASCE 7–10 establishes an interstory drift limit that depends on the structural system and the occupancy category of the building. For the MRF of the case-study building the 2% limit is obtained, at a hazard level compatible to current codes i.e. 10%/50yrs. Even though 10%/50yrs refers specifically to exceedance probabilities over a certain time period, its direct correspondence to the MAF will allow us to use this term interchangeably with actual MAF values, thus henceforth making 10%/50yrs identical to $-\ln(1-0.10)/50=0.0021$. Code-specific requirements do not employ limits on the system-level ductility capacities but they can be inferred following the process reported in NEHRP provisions (BSSC 2010). Specifically, the ductility capacity associated with the maximum strength of the intended mechanism for the design basis ground motion is multiplied by the 3/2 to obtain the corresponding limit for the 2%/50yrs hazard level (equivalent to $4.04{\cdot}10^{-4}$). The resulting ductility limit is $3.6/I_e=3.6$, where the I_e is the importance factor defined in ASCE 7–10 at the 2%/50 hazard level. For the case at hand, the critical PO that governs the structural design is the ductility demand. Since this design is compatible with current code provisions, the confidence level at which the POs should be met cannot be enforced directly, thus a 50% confidence is adopted for all the targeted POs.

5.3 Design of the MB and MC frames

The MB and MC frames are designed following the risk-based seismic design procedure introduced via the YFS. The main difference among the design of these two frames concerns the YFS generation. In the MC case, YFS are calculated by employing site-specific hazard data, while for the MB frame a simplified approach is adopted, indicative of what can be done for cases where site-specific information is not available. Specifically, for MB the 10%/50yrs UHS for site class D is used as a basis. Per ASCE (2010) this is taken as 2/3 of the corresponding smoothed 2%/50yrs UHS. To obtain the seismic intensities for other hazard levels, we follow the power law fit (or linear fit in log-space) concept of Cornell et al. (2001), using separate approximations below and above the 10%/50yrs level. A scale factor equal to 1.5 (i.e., the inverse of 2/3) naturally transforms the 10%/50yrs UHS to the 2%/50yrs one, while the UHS for the 50%/50yrs hazard level is derived by employing the scale factor of 0.5, as proposed by EN1998-1 (CEN 2005). These three data points at 50, 10, and 2% in 50 years allow us to linearly interpolate and extrapolate in log-space to approximate all other hazard levels. A second-order approximation of the hazard curve may also be employed (Vamvatsikos 2014), yet this may not be commensurate with the reduced accuracy provided by the three approximate hazard points, thus it is not adopted herein.

The MB frame is designed by targeting a single PO that is limiting the MAF of exceeding the maximum (over all stories) interstory drift ratio, θ_{max}, of 2% to 0.0021 (or a 10%/50yrs hazard level) at 68% confidence. This confidence level is selected to be higher than the 50% sought for the MA frame so as to obtain a more stringent design.

The MC frame is designed for three POs: (i) limiting the MAF of exceeding a system ductility demand of 1.50 to 0.0139 (equivalent to 50%/50yrs), this ductility limit being equivalent to a roof drift ratio of 0.09 m·1.5/16.5 m = 0.8%, where 0.09 m is the effective yield displacement and 16.5 m is the height of the building; (ii) limiting the MAF of exceeding θ_{max} = 2% to 0.0021 (equivalent to 10%/50yrs); (iii) limiting the MAF of reaching the Global Collapse limit state to $2.01 \cdot 10^{-4}$ (equivalent to 1%/50yrs). An appropriate level of confidence is chosen for each PO by considering the consequences of the EDP capacity exceedance, thus the confidence level associated with collapse is set at 90% while for the other two POs at 70%. It should be noted that global collapse occurs when either numerical non-convergence appears in a model that incorporates material and geometric nonlinearities or a large value of θ_{max} is exceeded, whichever occurs first. Herein the θ_{max} threshold indicating collapse is taken as 8%; actually any value higher than about 5% is equally effective in determining collapse, at least for this structure, as later results will show. Consequently, for this PO θ_{max} is adopted as the EDP.

The critical PO that governs the design of the building, at least when determining the YFS, is collapse. Note that for MC, the YFS are generated by adopting the mean estimate of the seismic hazard of the San Jose site, as derived by the USGS data. Note how this implies that any (expectedly minor) mismatch between the actual hazard and its approximation by ASCE 7–10 will be reflected in the design. Still, this is a valid representation of how such design approaches would be employed in practice. For more clarity, the salient characteristics of all design approaches are summarized in Table 1.

As a postscript, note that both MB and MC MRFs may require iteration to achieve their objectives, given that performance is verified by rigorous assessment after a design cycle. There are multiple factors that can lead to needing several design-iteration cycles, especially any discrepancy in assessing the yield displacement and ultimately representing a building by its equivalent SDOF proxy. At least for this simple four-story building, the YFS approach allowed fulfilling all design objectives without iteration. This is a feat that may not be observed for taller or irregular 3D structures, yet it is indicative of the good convergence properties of YFS.

Table 1 Salient characteristics of the five design approaches. Approaches CA and CB differ only on the member sizing approach, CB using the lightest possible sections, while CA adopting less optimal sections, closer to practice

Approach	Basis	Invariant	Tool	Hazard
CA/CB	Intensity	T	Code R-factors	10/50yrs code spectrum
MA	Intensity	δ_y	YPS	10/50yrs code spectrum
MB	Risk	δ_y	YFS	10/50yrs code spectrum*
MC	Risk	δ_y	YFS	Full site hazard

*With approximate scaling factors to extend to other hazard levels

5.4 Dimensions and reinforcement ratio for all design approaches

The cross-sectional dimensions and longitudinal reinforcement for beams and columns are presented in Table 2 for all frames. The format used for describing the reinforcement is (number of steel rebars) #(rebar number). It should be noted that the column reinforcement ratio for the CA and CB moment frames is distributed along the two edges parallel to the column width and does not include any additional reinforcement used for satisfying detailing requirements, while the longitudinal reinforcement of the MA, MB, and MC MRFs is distributed around the perimeter of the columns. This has to do with the assumptions adopted by the designers of the two frames. The terms "end" and "intermediate" columns are used to distinguish among the external and internal columns of each MRF as presented in Fig. 1a. For some columns that have different reinforcement at the top and the bottom, two values are written in the Table 2 that are separated by a slash "/". It should be noted that for the MA, MB, and MC frames the reinforcement is directly calculated based on the mathematical solutions behind fulfilling the V_y^* demand (Aschheim et al. 2019), without accounting for other detailing requirements, such as the minimum allowable distance between the rebars. For comparison purposes, the total concrete volume and steel weight of the designed MRFs (not the entire building) are also presented. It can be observed that the amount of steel and concrete required for the MRFs progressively increases for the CA/CB, MA, MB and MC MRFs, i.e., there is a tradeoff between economy and safety as more comprehensive performance objectives that are sought during the design tend to lead to increased amounts of steel and concrete.

6 Seismic performance assessment

The seismic performance of the five buildings is assessed to examine whether they satisfy the POs targeted either explicitly (e.g., collapse for the MC frame) or implicitly (e.g., collapse for all other frames) and to compare their performance for the POs that they share. Herein the additional uncertainty is considered equal to 0.25 for all design approaches.

6.1 Seismic hazard

The seismic hazard for San Jose is derived through the USGS data for a wide range of intensity levels and periods that can be pertinent to the designs. Accordingly, the spectral acceleration at the fundamental period of the building, $Sa(T)$, is adopted as the IM. The resulting 10%/50yrs UHS is shown in Fig. 2. Such data represents the actual seismicity of the site, as required for accurate performance assessment or risk-based design a la MC. However, design approaches CA, CB, MA and MB are based on code spectra rather than the site-specific UHS, thus the inevitable (minor) discrepancies that exist between the design spectrum (solid line) and the true UHS (dash-dotted line) may introduce inconsistencies and unfairly bias our evaluation of the simpler approaches.

To provide a fair basis for judging the capabilities of design approaches CA, CB, MA, and MB, which use the code spectrum as a basis, the site-specific seismic hazard curve is uniformly scaled to match the $Sa(T_1)$ value implied by the ASCE 7–10 design spectrum for each frame. For illustrative purposes, the modified UHS for the MB MRF is presented in Fig. 2; it is derived by scaling the site-specific UHS by 0.91 so that it matches the

Table 2 Sizing of beams and columns of the moment-resisting frames, reinforcement, total steel volume and total concrete mass per frame for all design approaches

Design approach	Story	End columns†			Intermediate columns†			Beams				Steel mass (tn)	Concrete volume (m^3)
		width (in)	height (in)	bars‡	width (in)	height (in)	bars‡	width (in)	height (in)	top bars	bottom bars		
CA	1	30	30	24 #9	30	40	18 #10	24	42	10 #9	8 #9	17	131
	2	30	30	16 #9	30	33	24 #9	24	36	9 #9	7 #9		
	3	24	28	14 #8	30	34	16 #8	24	32	7 #9	5 #9		
	4	24	28	14 #8	30	34	16 #8	24	32	6 #9	4 #9		
CB	1	30	30	24 #8	30	36	26 #9	24	36	10 #9	8 #9	16	112
	2	30	28	18 #8	30	30	22 #8	24	30	10 #8	6 #8		
	3	24	26	12 #8	30	30	14 #8	24	26	9 #8	5 #8		
	4	24	26	12 #8	30	30	14 #8	24	24	7 #8	4 #8		
MA	1	36	36	16 #10	36	36	36 #10/24 #10	24	36	16 #9	10 #8	24	114
	2	32	32	16 #10	32	32	24 #10	24	36	16 #9	9 #8		
	3	30	30	16 #10/12 #10	30	30	24 #10/20 #10	18	32	12 #9	7 #8		
	4	26	26	12 #10	26	26	20 #10	14	22	6 #9	3 #8		
MB	1	36	36	24 #10/20 #10	36	36	40 #10/32 #10	22	38	18 #9	9 #9	29	120
	2	36	36	20 #10	36	36	32 #10	22	36	18 #9	8 #9		
	3	32	32	20 #10	32	32	28 #10	20	32	14 #9	6 #9		
	4	28	28	12 #10	28	28	20 #10	14	24	7 #9	3 #9		
MC	1	38	38	20 #10/24 #10	38	38	48 #10/36 #10	26	42	22 #9	10 #9	35	146
	2	38	38	24 #10	38	38	36 #10	26	42	20 #9	10 #9		
	3	34	34	24 #10	34	34	36 #10	22	36	16 #9	8 #9		
	4	30	30	20 #10	30	30	28 #10	16	28	10 #9	5 #9		

†The end and intermediate columns for the frames are presented in Fig. 1a

‡longitudinal rebars not including additional reinforcement used for supporting stirrups and to satisfy minimum rebar distance requirements. In the CA and CB MRFs the rebars are placed along the two edges of the column, acting in the strong beam direction when the frame deforms in plane. For the MA, MB, and MC frames the bars are uniformly distributed around the perimeter of the column

ASCE 7–10 smoothed design spectrum at the fundamental period of the MB building that is 0.97 s. Such scaling is not needed for the MC frame since its design is already based on site-specific hazard data.

6.2 Non-linear modeling of the MRF

The OpenSees platform (McKenna et al. 2000) is used for preparing the two-dimensional (2D) model of the building for each design approach. In all cases, only one out of the two MRFs acting in each principal direction is modelled. A leaning column is added to model the effect of the gravity columns of one half of the building, i.e., those that do not belong to the MRF; it is pinned at the foundation and employs linear elastic elements. Two 2D-models are prepared for each building, one with distributed-plasticity elements and another with lumped-plasticity ones. The former accurately predicts the structural response at lower intensities, since it can capture phenomena such as concrete cracking and the gradual plastification of sections. On the contrary, the lumped-plasticity model can better reproduce the post-capping behaviour of the structure, but at the same time it cannot easily capture the pre-yield segment. Still, it is far less complex and numerically more robust, thus there is incentive in employing a lumped-plasticity model that is also reasonably accurate in the pre-yield segment for all dynamic analyses.

6.2.1 Distributed-plasticity model

The beams and columns of the distributed-plasticity model are realized as force-based elements that are discretized into longitudinal steel and concrete fibers. The fiber section representation is monitored at five integration points along the member length. The unconfined concrete of the cover is modelled via a uniaxial nonlinear law (Concrete01 in OpenSees) proposed by Kent and Park (1971) and Scott et al. (1982), and the confinement-related parameters are calculated for the concrete core on the basis of Mander et al. (1988). The steel rebars are modeled by employing a bilinear constitutive law that accounts for pinching and stiffness degradation. It should be noted that for performance assessment the material strengths are set at their expected values rather than their nominal characteristic strengths, i.e., f_{ce} = 6.5ksi (45 MPa) for the concrete and f_{ye} = 69ksi (476 MPa) for the steel reinforcement.

The rigid diaphragm is simulated by employing horizontal stiff truss elements connecting all the beam-column joints at each floor level. In addition, low-stiffness axial "buffer" springs are added to connect one end of each beam to the column. These allow the beams to stretch axially, removing the condition of zero axial strain that would normally result from applying rigid kinematic constraints on both beam ends; these would otherwise result in fictitious axial compressive forces that would artificially increase the beams' moment-rotation capacity (e.g., see Barbagallo et al. 2020).

6.2.2 Lumped-plasticity model

In the lumped-plasticity model, the beams and columns are modelled using a single force-based beam-column element per member with concentrated plastic hinges at both ends. The moment-rotation relationship for each hinge is based on the generalized backbone curve of ASCE/SEI 41–13 (ASCE 2013), originally defined as piecewise linear with five corner points: Point A is at the origin, B at yield, C at maximum strength (capping), D at

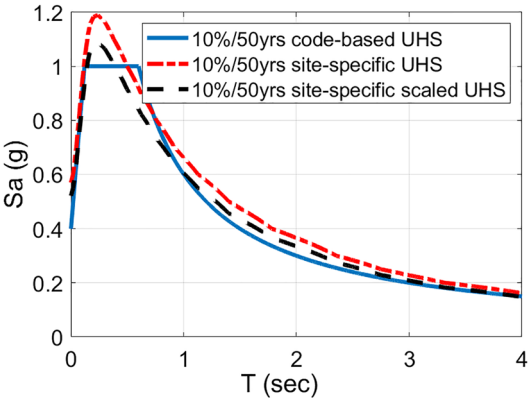

Fig. 2 The 10%/50yrs UHS for San Jose (red dash-dotted line) plotted against the corresponding ASCE 7–10 design spectrum (blue solid line). The modified UHS for the MB frame (black dashed line) is produced by uniformly scaling the site-specific UHS (red dash-dotted line) to match the Sa(0.97 s) value of the code spectrum

the start of the residual plateau, and E at ultimate failure. The moment at point B is approximately estimated through moment–curvature analysis of the actual fiber section instead of using respective formulas. For the moment–curvature analysis, the axial force is set equal to zero for the beams and equal to the gravity loads for the columns. ASCE/SEI 41–13 acceptance criteria for Immediate Occupancy (IO), Life Safety (LS) and Collapse Prevention (CP) are employed for all the beams and columns of the five moment-frames (see also Aschheim et al. 2019).

Regarding the initial stiffness of beams and columns, the code typically suggests reducing the gross stiffness properties to account for concrete cracking. For instance, ASCE-SEI 41–13 adopts the $0.3EI_g$ approximation for non-prestressed concrete beams and 0.3 or $0.5EI_g$ for concrete columns, depending on the level of the design axial load acting on the member, where E is the Young's modulus of concrete and I_g is the moment of inertia of the gross section. However, such conservative estimates may introduce inaccuracies in cases where unbiased results should be sought, such as in performance-based seismic design or in performance assessment. For this reason, the elastic stiffness of the internal part of each beam-column element is modified so that the pre-yield behaviour of the lumped-plasticity model better matches that of the distributed-plasticity model. Specifically, the moment of inertia employed in beams and columns is set equal to the average of the initial "uncracked" stiffness and the nominal "cracked" stiffness at yield, as derived by moment–curvature analysis.

This modification of individual member stiffness allowed for better matching the period and stiffness of the lumped and distributed plasticity models. A comparison of the fundamental periods of the lumped-plasticity models employing section-based member stiffness versus the distributed-plasticity ones appears in Table 3. Although the lumped-plasticity models still retain somewhat higher periods, they match well enough the effective (rather than the initial) period of the distributed plasticity model. This is surely expected to reduce discrepancies in model response at low-to-moderate levels of deformation. Furthermore, as discussed in De Luca et al. (2013), a closer matching of periods is conducive to achieving better overall accuracy in performance assessment, even close to near-collapse.

The pushover curves of the distributed-plasticity and the lumped plasticity models are shown in Fig. 3 for all design approaches. The effect of the stiffness modification is obvious in the matching of the pre-yield segments of the pushovers, although for the CA and CB cases the drift at yield is slightly underestimated. It should be noted that the difference

in the post-yield hardening of the code-based versus the section-based lumped plasticity models is attributed to the modified stiffness of the members in the latter as a result of the calibration process. In addition, the distributed plasticity model does not incorporate some definite loss of strength or limiting deformation/rotation in its members, as it is only meant to be used for calibration in the pre-yield range. The resulting OpenSees models for all frames can be found in Chatzidaki (2022). Furthermore Fig. 4 compares all design approaches in terms of the static pushover capacity curve of the final lumped-plasticity model (with stiffness based on section analysis). First of all, the results clearly support the constant yield displacement hypothesis (Aschheim 2022). Actually, all five capacity curves look like scaled versions of each other, having more or less the same yield, capping, and ultimate points, but different base shear strengths. As expected, the ultra-optimized frame CB is inferior to all, with the more realistic CA design following. Then come the MA/MB/MC designs, in that order, clearly showing the effect of stricter performance criteria, and perhaps of more accurate approaches to verify their fulfilment.

6.3 Performance assessment results

The final lumped-plasticity model of the structure is subjected to Incremental Dynamic Analysis (IDA, Vamvatsikos and Cornell 2002) to estimate the system's fragility curves. The far-field ground motion set of FEMA P-695 (FEMA 2009b) is used for the dynamic analyses; it comprises of 22 ground motions, each having two horizontal components, thus resulting in 44 accelerograms. Each time-history is individually applied to the 2D-model of the MRF to assess its performance. IDA results are characterized by two scalars: the IM, which represents the seismic intensity of the record, and the EDP, which monitors the structural response. For each design approach, we examine its ability (i) to fulfil the global POs targeted in the design, and (ii) to satisfy local member-level POs mandated by ASCE 41–13 as well as Global Collapse and $\theta_{max}=2\%$. In all cases, the IM is selected to be the 5% damped first-mode spectral acceleration, $Sa(T_1,5\%)$. The EDP adopted in each case depends on the PO that is examined. Specifically, when examining the deformation limits or Global Collapse θ_{max} is adopted; for checking the global ductility limit, the roof drift ratio, θ_{roof}, is used instead. Regarding the member-level EDPs, the plastic hinge rotations are recorded for beams and columns. For simplicity in checking, since the plastic hinge rotation capacities are not constant among the columns and beams of an MRF, the maximum demand to capacity ratio, *DCR*, is adopted as the pertinent EDP (Jalayer et al. 2007).

Table 3 Fundamental periods of the distributed-plasticity models ($T_{distributed}$) versus the lumped-plasticity ones with section-based stiffness (T_{lumped}) for all design approaches

Design approach	$T_{distributed}$ (s)	T_{lumped} (s)
CA	0.78	0.98
CB	0.96	1.20
MA	0.85	1.05
MB	0.79	0.97
MC	0.65	0.79

6.3.1 POs specific to MA, MB, and MC designs

The acceptability of the POs that were set when designing the MA MRF is firstly examined, i.e., the ductility limit of 3.6 with a MAF threshold of 2%/50yrs (or equivalently $4.04 \cdot 10^{-4}$) and $\theta_{max} = 2\%$ with a MAF threshold of 10%/50yrs (or equivalently 0.0021). A confidence level of 50% is adopted for both POs as implicitly assigned during the design. The resulting MAF of exceeding $\theta_{max} = 2\%$ equals 0.0018 that is lower than the MAF threshold of 0.0021, thus this PO is successfully met. On the contrary, MA fails to satisfy the ductility capacity limit as the MAF of exceeding this PO is estimated at $9 \cdot 10^{-4}$ that is higher than the MAF threshold of $4 \cdot 10^{-4}$. To the extent that we may generalize, this indicates that intensity-based design approaches can fail to conform with targeted limit states, especially when one seeks acceptable performance beyond the LS territory where the corresponding uncertainties become substantial.

For the MB MRF the acceptability of $\theta_{max} = 2\%$ is examined at 68% confidence, with the resulting MAF being 0.0015, which is lower than the MAF threshold of 0.0021. Thus, this explicitly-targeted PO is successfully met, as shown in Table 4. Regarding the MC MRF, three different POs were targeted during design. The ductility limit of 1.5 and the $\theta_{max} = 2\%$ threshold are easily met (Table 4). The Global Collapse limit-state merits some careful discussion. The IDA analysis results in terms of $Sa(T_1,5\%) - \theta_{max}$ are presented in Fig. 5, where the grey circles show the values indicating collapse that are used to estimate the corresponding fragility curve. In our case, its median value equals 1.86 g and the dispersion (or log-standard deviation) is 33%. First, note that any θ_{max} value higher than 5% can be employed as a nominal collapse threshold, as all IDAs have practically flatlined. Second, the resulting MAF of exceeding collapse is $6 \cdot 10^{-4} > 2.01 \cdot 10^{-4}$, thus this PO does not seem to be satisfied.

However, it is important to consider that the simple amplitude scaling of IDA as well as the $Sa(T_1,5\%)$ adopted as the IM may not allow capturing the appropriate spectral shape of high intensity ground motions (Baker and Cornell 2006; Luco and Bazzurro 2007); this typically results in conservative MAF estimates for Global Collapse (Dávalos and Miranda 2019). For this reason, the spectral shape factor of FEMA P-695 (FEMA 2009a) can be employed to adjust the median of the collapse fragility upwards. For instance, for a system ductility estimated at the point of 20% loss of maximum strength per the MC capacity curve of Fig. 3, i.e., for $\mu = \delta_{u(80\%Vmax)}/\delta_{y,eff} = 0.52$ m/0.09 m = 5.8, period $T_1 \approx 0.80$ s, and assuming Seismic Design Category D_{max}, Table 7-1b of FEMA P-695 suggests $SSF = 1.34$. The adjusted Global Collapse fragility has a median value of 1.34•1.86 g = 2.49 g and retains the same log standard deviation of 33%. This results in an improved MAF estimate of 0.00019, which now meets the PO of 0.000201. Of course, better methods can be followed for achieving an unbiased assessment for Global Collapse (e.g., Lin et al. 2013; Kohrangi et al. 2017) or for any other POs where higher accuracy is sought. For our purposes, though, the FEMA P-695 approach is adequate, especially since it was based on the same ground motion set employed herein as well as similar California sites.

6.3.2 POs shared by all designs

For all design approaches we shall examine in a uniform manner the acceptability of plastic hinge rotations for IO, LS and CP limit states, for $\theta_{max} = 2\%$, and for Global Collapse, aiming to test the performance of different design approaches along common criteria.

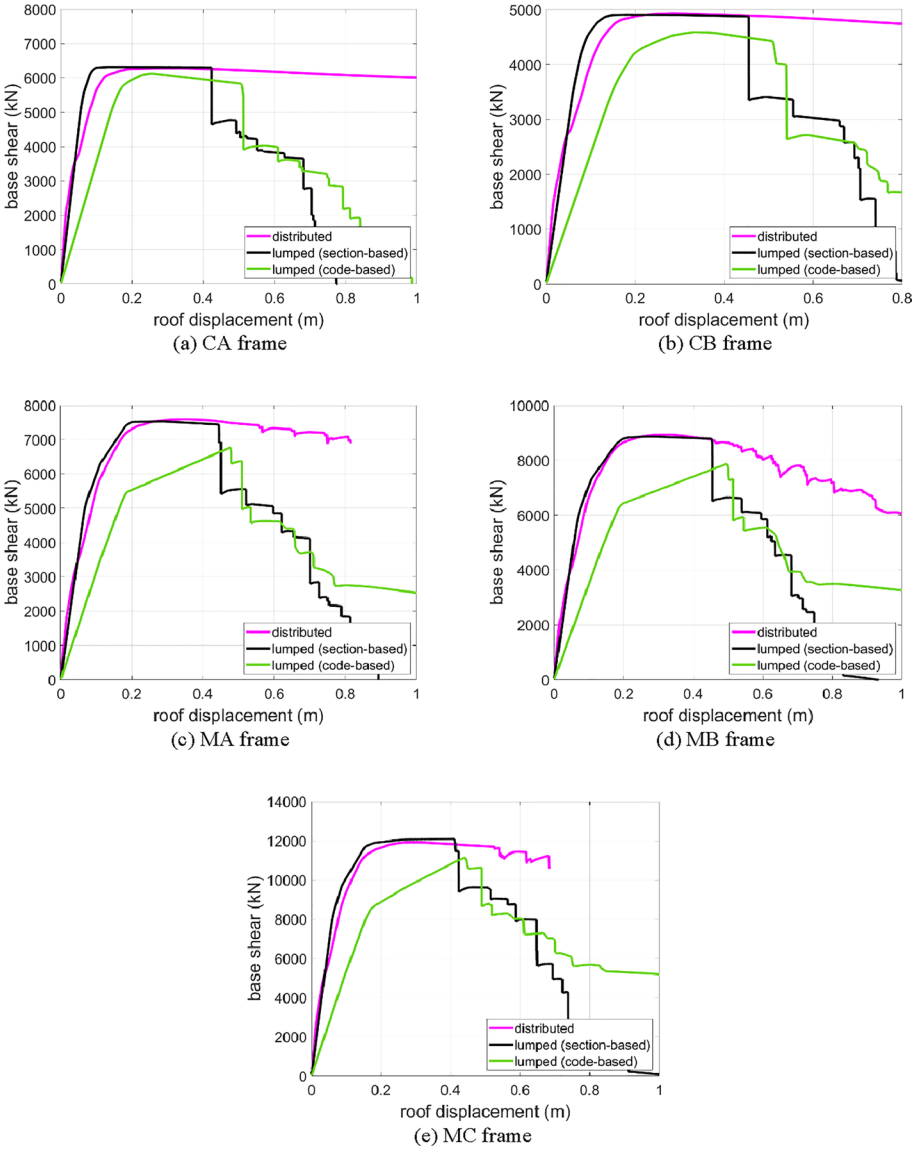

Fig. 3 Static pushover capacity curves using a first-mode load pattern for all design approaches for the distributed- and the lumped-plasticity models. For the latter, results for code-based element stiffness versus section-based element stiffness are shown. The effect of using section analysis to determine the initial stiffness is obvious in the matching of the pre-yield segments

For instance, the IDA results in terms of $Sa(T_1,5\%)$—DCR for beams are shown in Fig. 6 for LS and the MA frame. The MAF of exceeding $DCR = 1.0$, i.e. of demand exceeding capacity, is estimated by fitting a lognormal fragility curve to the $Sa(T_1,5\%)$ values corresponding to this DCR limit (grey points in Fig. 6). At a confidence level of 50%, the resulting exceedance MAF is 0.0017, i.e., lower than the limit of 0.0021. Such a confidence

Table 4 Acceptability of POs targeted in the design of the MA/MB/MC MRFs

Design approach	Limit-state Target MAF	$\theta_{max}=2\%$ 0.0021	Ductility = 1.5 0.0139	Ductility = 3.6 $4.04\bullet10^{-4}$	Global collapse† $2.01\bullet10^{-4}$
MA	Confidence	50%		50%	
	MAF	0.0018 ✓		$9\bullet10^{-4}$ ×	
MB	Confidence	68%			
	MAF	0.0015 ✓			
MC	Confidence	70%	70%		90%
	MAF	0.0009 ✓	0.0047 ✓		$6\bullet10^{-4}$ × $1.9\bullet10^{-4}$ ✓

†First value is as estimated, second value includes FEMA P-695 bias correction

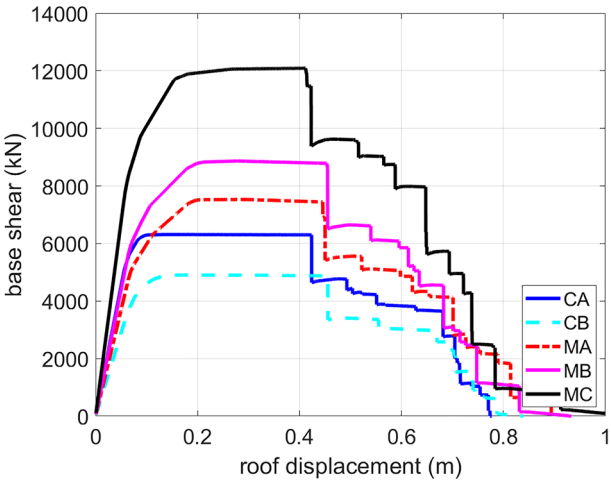

Fig. 4 Static pushover capacity curves of the lumped-plasticity models (section-based stiffness) for all design approaches

level essentially discards the effect of uncertainties. A stricter confidence of 70% would result in a MAF of 0.0024, which is higher than the limit of 0.0021, thus indicating failure to meet the PO. The maximum confidence where this PO is successfully met rests at 62%. For simplicity, the MAF value at 50% confidence together with the maximum achievable confidence level for success are presented in Table 5 for all POs. Indicatively, a bold typeface font is used to mark all those cases that cannot reach some common confidence limits, i.e., 90% for Global Collapse and 70% for all other limit states.

The CA frame, which by design exceeds the minimum code requirements, fails to pass Global Collapse but it successfully passes all other POs at 50% confidence. When stricter confidence levels are sought, it also fails to pass CP for beams and columns as well as $\theta_{max}=2\%$. The CB MRF, which meets the code requirements as closely as possible, at the 50% confidence level fails to pass Global Collapse and $\theta_{max}=2\%$, while the computed MAFs of exceeding CP for beams and columns nearly equal the target MAFs. When 70% confidence is sought instead, the MRF fails to pass CP for beams and columns, as well as LS for beams. The MA moment-frame successfully passes all POs at 50% confidence, while it fails to pass LS for beams and $\theta_{max}=2\%$ when 70% confidence is adopted, and

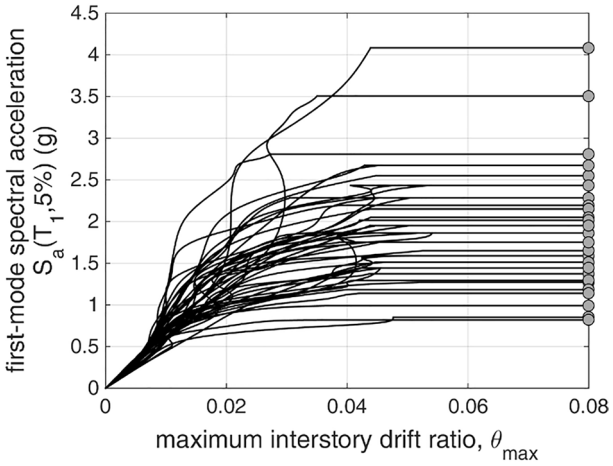

Fig. 5 IDA results of the MC frame in terms of $Sa(T_1,5\%)$—θ_{max} used for estimating the mean annual frequency of exceeding Global Collapse

Global Collapse at 90% confidence. In general, the success or failure at POs which were not specifically included in the design process is clearly a toss-up. For POs that are related to the design POs, one can expect a favorable outcome. For other less-related ones, such as the Global Collapse of MB, the comparison may end up either way. In this case, the result was unfavorable. By explicitly including said PO in the design of MC, this uncertainty was clearly removed. The MB MRF successfully passes all POs at 50% and 70% confidence, yet it fails to pass Global Collapse at 90%. In general, success or failure can be a toss-up for POs that were not explicitly included in the design process. For POs that are closely related to the design ones, we can expect a favorable outcome. For other less-related ones, such as the Global Collapse of MB, the comparison may end up either way. In this case, the result was unfavorable. By explicitly including said PO in the design of MC, this uncertainty is removed. Ultimately, only the MC MRF successfully passes all POs at all examined confidence levels.

7 Concluding remarks

Five different design approaches are compared for a 4-story moment-resisting frame building. Three of them offer code-compatible solutions, with the first two having been designed on an intensity&force-basis, while the third is designed by employing an intensity&displacement-based procedure via the YPS. The remaining two follow a performance/displacement-based design via the YFS to offer solutions that can satisfy any set of predefined POs.

When performance assessment is performed on the five designs, all intensity-based designs fail to meet Global Collapse POs and maximum interstory drift limits. Still, they largely meet IO, LS and CP objectives for beam and column rotations, especially when discarding the effect of additional uncertainties. On the contrary, performance-based approaches based on the YPS and the YFS allow designing structures that actually conform with pre-defined POs at the desired level of confidence without requiring many iterations during the design process as they rely on an initial estimate of the building's yield displacement that can be easily quantified if the geometry and material properties are known. Still,

Table 5 Exceedance MAFs for beam and column plastic hinge rotations, interstory drift ratio of 2%, and Global Collapse for all designs, estimated at the 50% confidence level. The maximum confidence that can be requested in achieving each PO is also noted inside the parentheses. A bold typeface font is used for all those cases that cannot reach 90% confidence for Global Collapse and 70% for other limit states

Design approach	Global collapse†	$\theta_{max}=2\%$	Beams			Columns		
			IO	LS	CP	IO	LS	CP
target MAF	$2.01\cdot10^{-4}$	0.0021	0.0139	0.0021	0.0010	0.0139	0.0021	0.0010
CA	**$6.96\cdot10^{-4}$/$2.52\cdot10^{-4}$ (40%)**	**0.0017 (62%)**	0.0040 (>99%)	0.0010 (84%)	**0.0008 (62%)**	0.0067 (94%)	0.0009 (88%)	**0.0008 (60%)**
CB	**$9.50\cdot10^{-4}$/$4.04\cdot10^{-4}$ (20%)**	**0.0027 (35%)**	0.0071 (94%)	**0.0015 (69%)**	**0.0010 (50%)**	0.0056 (98%)	0.0012 (82%)	**0.0010 (50%)**
MA	**$3.94\cdot10^{-4}$/$1.32\cdot10^{-4}$ (66%)**	**0.0018 (60%)**	0.0098 (80%)	**0.0017 (62%)**	0.0006 (75%)	0.0038 (>99%)	0.0005 (98%)	0.0004 (85%)
MB	**$2.96\cdot10^{-4}$/$0.92\cdot10^{-4}$ (77%)**	0.0011 (83%)	0.0080 (89%)	0.0009 (88%)	0.0004 (88%)	0.0029 (>99%)	0.0004 (98%)	0.0003 (92%)
MC	$1.68\cdot10^{-4}$/$0.46\cdot10^{-4}$ (91%)	0.0006 (95%)	0.0046 (>99%)	0.0004 (96%)	0.0002 (96%)	0.0035 (>99%)	0.0003 (>99%)	0.0002 (97%)

†First value is as estimated, second includes FEMA P-695 bias correction; displayed confidence corresponds to the latter value

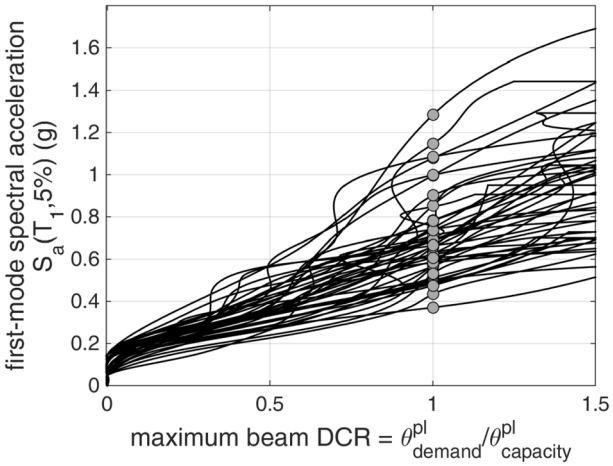

Fig. 6 IDA results in terms of $Sa(T_1,5\%)$—*DCR* used for estimating the mean annual frequency of exceeding $DCR=1$ for beam plastic hinge rotations at the LS limit state of the MA moment-frame

the aforementioned conclusions have only been tested on a 4-story building with regular plan and elevation; whether they hold for more complex structures and especially at limit states beyond LS territory is less certain. Still, we may derive some confidence in that such results concur with the conclusions reached by other prominent studies, such as by Sinković et al. 2016; Shahnazaryan and O'Reilly 2021; Shahnazaryan et al. 2022; Van der Burg et al. 2022; Gentile and Calvi 2023, who broadly agree that the effort expended in a performance/risk-based approach is generally rewarded by consistent conformance to the stated performance objectives, be they response or loss based. Naturally, tackling structures of higher complexity, at least for the YPS- and YFS-based approaches, would also increase

the effort in terms of design/analysis iterations due to the SDOF proxy employed in both methods. Still, it would not decrease the fidelity of the results thanks to the rigorous performance assessment used for the final design validation.

Acknowledgements The manuscript has benefitted from the guidance, diligence, and insights of Prof. Mark Aschheim, who performed the alternative designs of the buildings and assisted with the interpretation of the results. He was present from the very start, but unfortunately not the end of our work. We are forever indebted to him. The first author gratefully acknowledges the financial support provided by the Eugenides Foundation in Greece. Financial support has also been provided by the Hellenic Foundation for Research and Innovation (H.F.R.I.) under the "2nd Call for H.F.R.I. Research Projects to support Faculty Members & Researchers", Project "TwinCity: Climate-Aware Risk and Resilience Assessment of Urban Areas under Multiple Environmental Stressors via Multi-Tiered Digital City Twinning", (Number: 2515). Finally, the contribution of Fotis Andris and Charilaos Lyritsakis to the initial preparation of the models is gratefully acknowledged.

Author contributions All authors contributed to the study conception and design. Material preparation, data collection and analysis were performed by AC. The first draft of the manuscript was written by AC and DV and all authors commented on previous versions of the manuscript. All authors read and approved the final manuscript.

Funding Open access funding provided by HEAL-Link Greece. This work was supported by the Hellenic Foundation for Research and Innovation (H.F.R.I.) under the "2nd Call for H.F.R.I. Research Projects to support Faculty Members & Researchers", Project "TwinCity: Climate-Aware Risk and Resilience Assessment of Urban Areas under Multiple Environmental Stressors via Multi-Tiered Digital City Twinning", (Grant Number: 2515). Author Akrivi Chatzidaki has received financial support by the Eugenides Foundation in Greece.

Data availability The datasets generated during and/or analysed during the current study are available in http://users.ntua.gr/divamva/RCbook/Examples123_MatlabOpenSeesFiles.zip

Declarations

Conflict of interests The authors have no relevant financial or non-financial interests to disclose.

References

ASCE (2010) Minimum design loads for buildings and other structures. ASCE/SEI 7–10, American Society of Civil Engineers, Reston, VA

ASCE (2013) Seismic Evaluation and Retrofit of Existing Buildings. ASCE/SEI 41–13, American Society of Civil Engineers, Reston, Virginia

Aschheim M (2002) Seismic design based on the yield displacement. Earthq Spec 18(4):581–600. https://doi.org/10.1193/1.1516754

Aschheim M, Black EF (2000) Yield point spectra for seismic design and rehabilitation. Earthq Spec 16(2):317–335. https://doi.org/10.1193/1.1586115

Aschheim M, Hernández-Montes E, Vamvatsikos D (2019) Design of reinforced concrete buildings for seismic performance: practical, deterministic and probabilistic approaches. CRC Press. https://doi.org/10.1201/b19964

Bakalis K, Kazantzi AK, Vamvatsikos D, Fragiadakis M (2019) Seismic performance evaluation of liquid storage tanks using nonlinear static procedures. ASME J Pressure Vessel Technol 141(1):010902. https://doi.org/10.1115/1.4039634

Baker JW, Cornell CA (2006) Spectral shape, epsilon and record selection. Earthq Eng Struct Dyn 35(9):1077–1095. https://doi.org/10.1002/eqe.571

Barbagallo F, Bosco M, Marino EM, Rossi PP (2020) On the fibre modelling of beams in RC framed buildings with rigid diaphragm. Bul Earthq Eng 18(1):189–210. https://doi.org/10.1007/s10518-019-00723-z

BSSC (2010) Resource Paper 9: Seismic Design using Target Drift, Ductility, and Plastic Mechanism as Performance Criteria. NEHRP Recommended Seismic Provisions for New Buildings and Other Structures, Building Seismic Safety Council, Federal Emergency Management Agency, Report No. FEMA P-750

CEN (2005) Design of Structures for Earthquake Resistance-Part 1: General Rules, Seismic Actions and Rules for Building. Eurocode 8, European Comimitee for Standarization, Brussels

Chatzidaki A (2022) Reinforced concrete building seismic design examples Available at http://users.ntua.gr/divamva/RCbook/Examples123_MatlabOpenSeesFiles.zip

Chopra AK, Goel RK (2000) Building period formulas for estimating seismic displacements. Earthq Spec 16(2):533–536. https://doi.org/10.1193/1.1586125

Cornell CA (1968) Engineering seismic risk analysis. Bul Seismol Soc Am 58(5):1583–1606. https://doi.org/10.1785/BSSA0580051583

Cornell CA, Jalayer F, Hamburger RO, Foutch DA (2001) Probabilistic basis for the 2000 SAC/FEMA steel moment frame guidelines. J Struct Eng 128(4). https://doi.org/10.1061/(ASCE)0733-9445(2002)128:4(526)

da Silva AHA, Tsiavos A, Stojadinović B (2023) Ductility-strength and strength-ductility relations for a constant yield displacement seismic design procedure. Bull Earthq Eng 21:4449–4479. https://doi.org/10.1007/s10518-023-01683-1

Dávalos H, Miranda E (2019) Evaluation of the Scaling Factor Bias Influence on the Probability of Collapse Using Sa(T1) as the Intensity Measure. Earthq Spectra 35(2):679–702. https://doi.org/10.1193/011018EQS007M

De Luca F, Vamvatsikos D, Iervolino I (2013) Near-optimal piecewise linear fits of static pushover capacity curves for equivalent SDOF analysis. Earthq Eng Struct Dyn 42(4):523–543. https://doi.org/10.1002/eqe.2225

Dolsek M (2009) Incremental dynamic analysis with consideration of modelling uncertainties. Earthq Eng Struct Dyn 38(6):805–825. https://doi.org/10.1002/eqe.869

Ellingwood B, MacGregor JG, Galambos TV, Cornell CA (1982) Probability based load criteria: load factors and load combinations. J Struct Division 108(5):978–997. https://doi.org/10.1061/JSDEAG.0005959

FEMA (2009a) Quantification of Building Seismic Performance Factors. Report FEMA P-695, prepared by the Applied Technology Council for the Federal Emergency Management Agency, Washington, D.C

FEMA (2009b) FEMA P-695 Far field ground motion set Available at http://users.ntua.gr/divamva/RCbook/FEMA-P695-FFset.zip)

FEMA (2012) Next-generation building seismic performance assessment methodology. Report FEMA P-58, prepared by the Applied Technology Council for the Federal Emergency Management Agency, Washington, D.C

Fragiadakis M, Lagaros ND (2011) An overview to structural seismic design optimisation frameworks. Computers Struct 89(11-12):1155–1165. https://doi.org/10.1016/j.compstruc.2010.10.021

Franchin P, Pinto PE (2012) Method for probabilistic displacement-based design of RC structures. J Struct Eng 138(5):585–591. https://doi.org/10.1061/(ASCE)ST.1943-541X.0000492

Franchin P, Petrini F, Mollaioli F (2018) Improved risk-targeted performance-based seismic design of reinforced concrete frame structures. Earthq Eng Struct Dyn 47(1):49–67. https://doi.org/10.1002/eqe.2936

Gentile R, Calvi GM (2023) Direct loss-based seismic design of reinforced concrete frame and wall structures. Earthq Eng Struct Dyn 52(14):4395–4415. https://doi.org/10.1002/eqe.3955

Gokkaya BU, Baker JW, Deierlein GG (2016) Quantifying the impacts of modeling uncertainties on the seismic drift demands and collapse risk of buildings with implications on seismic design checks. Earthq Eng Struct Dyn 45(10):1661–1683. https://doi.org/10.1002/eqe.2740

Haselton CB, et al. (2008) An assessment to benchmark the seismic performance of a code-conforming reinforced-concrete moment-frame building. Report 2007/1, Pacific Earthquake Engineering Research Center, Berkeley, CA

Hernández-Montes E, Aschheim MA (2019) A seismic design procedure for moment-frame structures. J Earthq Eng 23(9):1584–1603. https://doi.org/10.1080/13632469.2017.1387196
Hernández-Montes E, Jalón ML, Chiachío J, Gil-Martín LM (2023) Yield displacement charts for performance-based seismic design. Bull Earthquake Eng 21:237–255. https://doi.org/10.1007/s10518-022-01534-5
Iervolino I, Spillatura A, Bazzurro P (2018) Seismic reliability of code-conforming Italian buildings. J Earthq Eng 22(sup2):5–27. https://doi.org/10.1080/13632469.2018.1540372
International Code Council (2003) International Building Code 2003, International Conference of Building Officials. Falls Church, VA
Jalayer F, Franchin P, Pinto PE (2007) A scalar damage measure for seismic reliability analysis of RC frames. Earthq Eng Struct Dyn 36(13):2059–2079. https://doi.org/10.1002/eqe.704
Kazantzi AK, Vamvatsikos D (2021) Practical performance-based design of friction pendulum bearings for a seismically isolated steel top story spanning two RC towers. Bul Earthq Eng 19:1231–1248. https://doi.org/10.1007/s10518-020-01011-x
Kent DC, Park R (1971) Flexural members with confined concrete. ASCE J Struct Division 97(7):1969–1990
Kohrangi M, Bazzurro P, Vamvatsikos D, Spillatura A (2017) Conditional spectrum based ground motion record selection using average spectral acceleration. Earthq Eng Struct Dyn 46(10):1667–1685. https://doi.org/10.1002/eqe.2876
Krawinkler H, Zareian F, Medina RA, Ibarra LF (2006) Decision support for conceptual performance-based design. Earthq Eng Struct Dyn 35(1):115–133. https://doi.org/10.1002/eqe.536
Liel AB, Haselton CB, Deierlein GG, Baker JW (2009) Incorporating modeling uncertainties in the assessment of seismic collapse risk of buildings. Struct Saf 31(2):197–211. https://doi.org/10.1016/j.strusafe.2008.06.002
Lin T, Haselton CB, Baker JW (2013) Conditional spectrum-based ground motion selection Part 1: Hazard consistency for risk-based assessments. Earthq Eng Struct Dyn 42(12):1487–1865. https://doi.org/10.1002/eqe.2301
Luco N, Bazzurro P (2007) Does amplitude scaling of ground motion records result in biased nonlinear structural drift responses? Earthq Eng Struct Dyn 36(13):1813–1835. https://doi.org/10.1002/eqe.695
Mander JB, Priestley MJ, Park R (1988) Theoretical stress-strain model for confined concrete. J Struct Eng 114(8):1804–1826. https://doi.org/10.1061/(ASCE)0733-9445(1988)114:8(1804)
McKenna F, Fenves GL, Scott MH (2000) Open system for earthquake engineering simulation. University of California, Berkeley, CA
Moehle JP (1992) Displacement-based design of RC structures subjected to earthquakes. Earthq Spectra 8(3):403–428. https://doi.org/10.1193/1.1585688
O'Reilly GJ, Calvi GM (2020) Quantifying seismic risk in structures via simplified demand–intensity models. Bul Earthq Eng 18(5):2003–2022. https://doi.org/10.1007/s10518-019-00776-0
O'Reilly GJ, Calvi GM (2019) Conceptual design in performance-based earthquake engineering. Earthq Eng Struct Dyn 48(4):389–411. https://doi.org/10.1002/eqe.3141
Priestley MJN (2000) Performance based seismic design. Bul New Zealand Soc Earthq Eng 33(3):325–346. https://doi.org/10.5459/bnzsee.33.3.325-346
Priestley MJN, Calvi GM, Kowalsky M, Powell DH (2008) Displacement based seismic design of structures. Earthq Spectra 24(2):555. https://doi.org/10.1193/1.2932170
Ravindra MK, Galambos TV (1978) Load and resistance factor design for steel. J Struct Division 104(9):1337–1353. https://doi.org/10.1061/JSDEAG.0004981
Ruiz-García J, Miranda E (2007) Probabilistic estimation of maximum inelastic displacement demands for performance-based design. Earthq Eng Struct Dyn 36(9):1235–1254
Scott BD, Park R, Priestley MJN (1982) Stress–strain behavior of concrete confined by overlapping hoops at low and high strain rates. ACI J 79(1):13–27
Shahnazaryan D, O'Reilly GJ (2021) Integrating expected loss and collapse risk in performance-based seismic design of structures. Bul Earthq Eng 19(2):987–1025. https://doi.org/10.1007/s10518-020-01003-x
Shahnazaryan D, O'Reilly GJ, Monteiro R (2022) On the seismic loss estimation of integrated performance-based designed buildings. Earthq Eng Struct Dyn 51(8):1794–1818. https://doi.org/10.1002/eqe.3638
Sinković NL, Brozovič M, Dolšek M (2016) Risk-based seismic design for collapse safety. Earthq Eng Struct Dyn 45(9):1451–1471
Sørensen JD, Kroon IB, Faber MH (1994) Optimal reliability-based code calibration. Struct Saf 15(3):197–208. https://doi.org/10.1016/0167-4730(94)90040-X

Vamvatsikos D (2014) Seismic performance uncertainty estimation via IDA with progressive accelerogram-wise latin hypercube sampling. J Struct Eng 140(8):A4014015
Vamvatsikos D, Aschheim MA (2016) Performance-based seismic design via yield frequency spectra. Earthq Eng Struct Dyn 45(11):1759–1778. https://doi.org/10.1002/eqe.2727
Vamvatsikos D, Cornell CA (2002) Incremental dynamic analysis. Earthq Eng Struct Dyn 31(3):491–514. https://doi.org/10.1002/eqe.141
Vamvatsikos D, Cornell CA (2006) Direct estimation of the seismic demand and capacity of oscillators with multi-linear static pushovers through incremental dynamic analysis. Earthq Eng Struct Dyn 35(9):1097–1117. https://doi.org/10.1002/eqe.573
Vamvatsikos D, Fragiadakis M (2010) Incremental dynamic analysis for estimating seismic performance uncertainty and sensitivity. Earthq Eng Struct Dyn 39(2):141–163. https://doi.org/10.1002/eqe.935
Vamvatsikos D, Kazantzi AK, Aschheim MA (2016a) Performance-based seismic design: avant-garde and code-compatible approaches. ASCE-ASME J Risk Uncertainty Eng Syst Part a: Civil Eng 2(2):C4015008. https://doi.org/10.1061/AJRUA6.0000853
Vamvatsikos D, Kazantzi AK, Aschheim MA (2016b) Performance-based seismic design: avant-garde and code-compatible approaches. ASCE-ASME J Risk Uncertain Eng Syst Part a: Civil Eng 2(2):C4015008. https://doi.org/10.1061/AJRUA6.0000853
Vamvatsikos D (2017) Performance-based seismic design in real life: the good, the bad and the ugly. In: Proceedings of the ANIDIS2017 Italian National Conference on Earthquake Engineering, Pistoia, Italy
Van der Burg L, Kohrangi M, Vamvatsikos D, Bazzurro P (2022) A risk-based evaluation of direct displacement-based design. Bull Earthq Eng 20:6611–6633. https://doi.org/10.1007/s10518-022-01447-3
Zareian F, Krawinkler H (2012) Conceptual performance-based seismic design using building-level and story-level decision support system. Earthq Eng Struct Dyn 41(11):1439–1453. https://doi.org/10.1002/eqe.2218